COLLEGE OF ENGINEERING

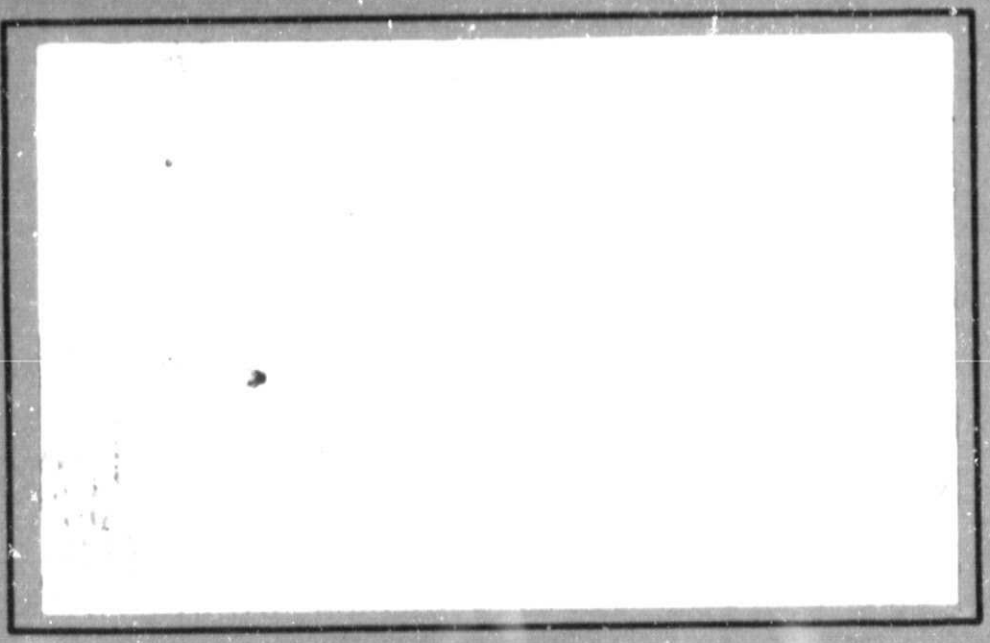

VIRGINIA POLYTECHNIC INSTITUTE AND STATE UNIVERSITY

BLACKSBURG, VIRGINIA

Semi-Annual Status Report
on
NASA Grant No. NAG 3-593

Thermodynamic Evaluation of Transonic Compressor Rotors Using the Finite Volume Approach

for the period
12/20/84 - 5/31/85

by
Stephen Nicholson
Instructor
and
John Moore
Professor of Mechanical Engineering
Principal Investigator

Grantee Institution -

NASA Lewis Research Center
21000 Brookpark Road
Cleveland, Ohio 44135

Turbomachinery Research Group

Report No. JM/85-6

Mechanical Engineering Department
Virginia Polytechnic Institute and State University
Blacksburg, Virginia 24061

EXTENSION OF A FINITE VOLUME EXPLICIT TIME MARCHING METHOD TO LAMINAR AND TURBULENT FLOW

ABSTRACT

This report documents progress made in extending the finite volume explicit time marching method to laminar and turbulent flow during the time period from January to May 1985. The work done is under NASA grant NAG 3-593. Previously, extensions had been made to the finite volume method to improve the accuracy of the calculation of total pressure in compressible inviscid flow. These changes are documented in reference 1 . The current work extends these ideas and develops new ideas which allow the calculation of laminar and turbulent boundary layers in internal flows. The method is verified using four test cases with free-stream Mach numbers ranging from .075 to 1.20.

GOVERNING EQUATIONS

The unsteady form of the continuity equation, the x-momentum equation, and the y-momentum equation, in integral form, are used to obtain a steady-state solution through 2-dimensional ducts by taking the limit of the unsteady solution as it approaches a steady value. The unknown variables are pressure, temperature, density, the x-component of the velocity, and the y-component of

the velocity. In addition to the continuity and momentum equations, we need an equation of state and the energy equation. The ideal gas equation of state is used. The energy equation currently reduces to the assumption of constant total temperature. These five equations are summarized in Table 1.

CONTROL VOLUMES

A new control volume has been introduced for this method[1]. To eliminate the need for the smoothing of flow properties, there must be as many control volumes across the duct as there are nodes where these variables are calculated. We need as many equations as unknowns. The control volumes also need to be located so that errors in continuity and momentum can correctly influence the changes in density and velocity without smoothing. The current control volume accomplishes this and is shown in Fig. 1. There are no nodes located along the wall. The nodes are located in the middle of the upstream and downstream faces of the control volumes. When calculating the flux through a streamwise face of an element, the values of the flow properties at the node on that face are used. When calculating the flux through a cross-stream face, first the properties are calculated at the corners of the element using linear interpolation, then the flux is calculated using the average of the flow properties at the ends of that face.

The control volumes used by Denton [2] look like those shown in Fig. 2. Fluxes of mass and momentum through each face are found by using averages of the flow properties stored at the ends

of each face, However, since the number of nodes (unknowns) is greater than the number of control volumes (equations), smoothing of flow properties is needed in the crossflow direction to remove the dependence of the final solution on the initial guess.

DISTRIBUTION OF PROPERTIES

The properties are changed in the flow field after each time step because the continuity and momentum equations are not satisfied for a given control volume. The amount that properties are changed at nodes depends upon the extent to which continuity and momentum are not satisfied, the volume of the control volume, and the time step. Changes in pressure are distributed to the upstream nodes based upon the continuity error. The equation for calculating the pressure change is

$$\delta P = RT\delta\rho \qquad (1).$$

where δP is the pressure change, R is the ideal gas constant, T is the local static temperature, and $\delta\rho$ is the density change calculated from the continuity error. This density change is not used to update the density directly but the density is updated at each node using the ideal gas equation of state,

$$\rho_x = (P_{x-1} + C_{x-1})/RT_x \qquad (2)$$

where P_{x-1} is the updated pressure.

The lagging correction factor C is defined as,

$$C_{I-1} = (1-F) \times C_{OLD} + F(P_I - P_{I-1}) \quad (3)$$

and is used to maintain stability as well as to assure that as the solution approaches a steady-state the ideal gas equation of state will be satisfied at each node. The relaxation factor, F, is typically 0.05 and the correction factor is updated every 10 iterations. It was found that the correction factor must not be updated after every step or the solution will become unstable. After the pressure is calculated, the momentum equations are solved for the changes in velocity. These changes in velocity are sent to the downstream nodes. These velocity changes are calculated from the momentum error using the updated pressures and the old densities and velocities. Finally the static temperature is updated using the energy equation.

When calculating the momentum fluxes, the $\rho\vec{V}\cdot\nabla\vec{V}$ form of the governing equations is approximated by using,

$$\nabla\cdot\rho\vec{V}\vec{V} - \vec{V}(\nabla\cdot\rho\vec{V}) \quad (4)$$

This form subtracts off the continuity error contribution to the momentum error and helps the stability characteristics of calculations with long thin control volumes. For more details, see reference 1.

BOUNDARY CONDITIONS

Along the upstream boundary, the total temperature, total pressure, and v-velocity are specified for inviscid flow. Along the downstream boundary the static pressure is specified. Pressures along the solid boundaries are determined from linear extrapolation. There is no mass flux across element faces which coincide with the solid boundaries.

For viscous flow, the values of the x-component and y-component of velocity are set equal to zero at solid walls. The inlet velocity profile is specified along with a freestream total pressure.

INITIAL GUESS

The initial guess for the inviscid part of the flow field is determined from a 1-D inviscid solution. A boundary layer is then added along the wall using a constant ratio of boundary layer thickness to duct height throughout the duct. The velocity profile used in the boundary layer is the inlet velocity profile. For certain geometries, an estimate of the blockage effect of the boundary layer is used to specify an effective geometry for the calculation of the initial solution.

TIME STEPS

As outlined in [1], different time steps are used for calculating the changes in pressure and velocities. Since we are only interested in the steady solution not only can we use different time steps at different nodes but also for different equations. If viscous terms are included, the time steps change because of the addition of a coefficient from the viscous term. The time step is reduced for the calculation of viscous flows. The resulting time or iteration step for the momentum equations is

$$\Delta t_m \leq \frac{1}{\left|\frac{u}{\Delta x}\right| + \left|\frac{v}{\Delta y}\right| + \left|\frac{\mu_{eff}}{\rho \Delta y^2}\right|} \qquad (5)$$

and for the continuity equation the iteration step is,

$$\Delta t_c \leq \frac{1}{RT\left[\left|\frac{\Delta t_m}{\Delta x^2}\right| + \left|\frac{\Delta t_m}{\Delta y^2}\right| + \left|\frac{u}{RT\Delta x}\right| + \left|\frac{v}{RT\Delta y}\right|\right]} \qquad (6).$$

In the actual calculations, the time steps are divided by 2 to 4 because the governing equations are non-linear.

A simple example can be used to explain in a qualitative sense why these different time steps are needed in the calculations. The continuity error results in a change in pressure at the upstream node associated with a control volume. This new pressure is then used in the momentum equation and produces a momentum change to improve the continuity error. But it can be observed that as the Mach number of the flow decreases a given percentage change in pressure produces an increasingly

larger change in velocity. The time step used to update the pressure must be reduced to keep the changes in velocity stable. Table 2 has a comparison of the ratio of velocity change to pressure change with the ratio of time steps calculated using equations 5 and 6 for various Mach numbers. The quantitative agreement of these explains the necessity of different time steps for the different equations using the current updating scheme. These numbers are calculated for 1-D compressible flow.

For low Mach number flows, the time step used in the momentum equation can be much greater than that specified by the CFL condition. In some of the calculations to be discussed later, the time step used in the momentum equation was 500 times the CFL condition. While the time step used for continuity was much less than the time step specified by the CFL condition.

CALCULATION OF VISCOUS STRESSES

The viscous shear stresses are calculated using the following equation,

$$\tau = \mu_{eff} \frac{du}{dy} \qquad (7)$$

where μ_{eff} is the effective viscosity, and du/dy is the local velocity gradient. For laminar flow the effective viscosity is the absolute viscosity. For the turbulent flow, the viscosity is calculated using a Prandtl mixing length model. The equations used are summarized in Table 3. Between the near wall point and the wall a velocity gradient is calculated and an effective

viscosity is calculated at the midpoint using $\mu_{eff} = \sqrt{\mu_l(\mu_l+\mu_T)}$ [3]. The shear stress at the wall is then calculated from this velocity gradient and this effective viscosity. By using this effective viscosity, accurate results have been obtained using a near wall point at a y+ greater than that usually required . A typical value for y+ at the near wall point used in the test cases is 30.

For a non-uniform grid, the top and bottom faces of the control volume are not midway between the grid points. The velocity gradient calculated from the velocities at the nodes and from the distance between these nodes is only valid midway between the grid points. In the calculations, the mixing length is calculated midway between the points and the shear stress is then calculated using this mixing length and the calculated velocity gradient. This shear stress is then assigned to the face of the control volume between the points. Fig. 3 shows schematically the ideas just discussed. This procedure is used because the mixing length varies more rapidly than the shear stress through the boundary layer .

NON-UNIFORM GRID SPACING

For the calculation of internal flows, a numerical algorithm must be able to calculate the effect of thin boundary layers which grow along the walls of the duct. To be able to calculate this type of flow field with a reasonable number of grid points, a non-uniform grid must be used with larger spacing in the freestream and a higher density of grid points near the walls of

the duct. Fig. 4 shows how the grid points and control volumes might look as you approach the walls of the duct using non-uniform grid spacing. The key thing to notice is that the aspect ratio (length/height) of the control volumes becomes larger as you approach the wall. In the finite-volume formulation, this type of control volume requires special treatment to maintain the stability of the scheme.

A more non-uniform grid is needed when calculating a flow with turbulent boundary layers since the velocity gradients near the wall are much larger. In the present calculations , in the boundary layer region, the height of each successive control volume is reduced by 50% as the grid approaches the wall. Typical distributions of grid points are shown in Table 4 for the laminar and turbulent flow calculations. In both cases, the boundary layer is only calculated along one wall of the duct.

A MULTI-VOLUME METHOD FOR PRESSURE CHANGES IN THE BOUNDARY LAYER

Preliminary calculations of boundary layer flows resulted in solutions which became unstable after only a small number of iteration steps. After a detailed investigation of the nature of this instability, the cause could be attributed to effects resulting from the large aspect ratio of the control volumes. The first contributing factor was the use of different time steps for each control volume and each equation. The time steps that were to be used for calculating the change in the density were very small. The ratio of the momentum and continuity time steps was also very large. The changes in pressure were proceeding in a

direction which led to large cross velocities and an unstable calculation procedure. It was felt that to stabilize this calculation procedure, the changes in pressure through the boundary layer must be coupled in some manner and that the changes in pressure be only dependent on the continuity error and not on both the density change through the continuity error and the temperature change through the momentum error and its resulting velocity change.

The above realizations resulted in two changes. The first change altered the way that the continuity error is used to update the flow properties. Previously [1], errors in continuity were used to update the density at the node points. The pressure was then calculated from the equation of state. An alternative procedure has been developed which updates the pressure directly from the equation of state (Eqn. 2). To maintain stability, a lagging correction factor (Eqn. 3) is used in Eqn. 2 for determining the effective pressure to be used in calculating the density at a point. In the limit as the solution reaches steady state, the density is evaluated using the correct pressure. This procedure is used throughout the flow field and is stable for both subsonic and supersonic Mach numbers.

The second change is to group control volumes in the boundary layer to form a larger global control volume. The continuity error is calculated for this global control volume and changes in pressure are assigned equally to each of the upstream nodes. Initially the global control volume extends from the wall to the edge of the boundary layer. Then the global control volume is made successively smaller towards the wall. This is shown

schematically in Fig. 5. A continuity time step is calculated for each global control volume based upon the average properties for the control volume.

TRANSVERSE UPWIND DIFFERENCING

When the control volumes become long and thin near the wall of the duct, the fluxes through the top and bottom faces of the control volume become more significant in comparison to the fluxes through the streamwise faces. Because the nodes of the control volumes are located in the middle of these streamwise faces, the predominant flow direction must be in the streamwise direction for the discretization method described earlier (see Control Volumes) to properly reflect the convective nature of the flow. When the fluxes in the transverse direction become significant, the solution procedure may become unstable because the diagonal terms in the coefficient matrix become smaller as the transverse fluxes increase. This is due to the fact that the velocities at the corners of the nodes are determined from interpolation. To strengthen the diagonal dominance of the coefficient matrix, the momentum fluxes through the transverse faces are calculated using the velocities upstream in the transverse direction rather than the interpolated values. These velocities are multiplied by the mass fluxes through the sides of the control volumes to get the total momentum flux. The direction of the upwinding is determined from the sign of the continuity flux for each face . In the calculations discussed below, this upwinding was needed only in the diverging portion of the ducts.

TEST CASES

Four test cases have been used so far to test the accuracy and stability of the method described in the beginning of this progress report. The test cases are of increasing difficulty and each serves as a useful check on the method's accuracy. The test cases are:

1. laminar boundary layer in an essentially zero pressure gradient.
2. laminar boundary layer in a favorable pressure gradient.
3. incompressible turbulent boundary layer in an adverse pressure gradient.
4. compressible turbulent boundary layer in a transonic diffuser.

These test cases will now be discussed individually in more detail.

TEST CASE #1

A laminar boundary layer was calculated in a constant height duct. The boundary layer thickness at the inlet was 15% of the duct height. The freestream Mach number was 0.43. The inlet velocity profile was the Blasius profile. The absolute viscosity was 0.01 kg/m s. The duct height was 44 mm and the

duct length was 112 mm. The geometry and the grid are shown in Fig. 6. The Reynolds number based upon x varies from 5070 to 11840 along the duct. The duct is 17 inlet boundary layer thicknesses long.

Fig. 7 shows that the development of the velocity profile compares very well with that predicted by theory.

TEST CASE # 2

A laminar boundary layer was calculated in a converging nozzle. The boundary layer thickness was 15% of the inlet duct height. The inlet velocity profile was the Blasius profile. The inlet height of the duct was 44 mm and the exit height was 31 mm. The length of the duct was 112mm. The grid and the geometry are shown in Fig. 8. The absolute viscosity was 0.01 kg /m s. The inlet freestream Mach number is 0.43.

The calculated velocity profiles were compared with the Pohlhausen velocity profiles for the given freestream pressure gradients. The velocity profiles are compared at the inlet (lambda=0.0), midway along the duct(lambda=9.1), and the exit (lambda=2.0). These results are shown in Figs. 9,10, and 11 respectively. The agreement is good showing the effect of the favorable pressure gradient in changing the shape of the velocity profiles ;note that we should only expect qualitative agreement with the simple Pohlhausen approximation.

TEST CASE # 3

Incompressible turbulent boundary layer flow in a diverging duct was calculated for test case 0141 of the Stanford Conference (Samuel and Joubert)[4]. The geometry and grid used by Moore [3] are shown in Fig. 12. With this geometry, the top wall is treated as inviscid in the calculations. The inlet velocity is 26 m/s.

Fig. 13 shows a comparison of the calculated skin friction coefficient with the experimental results and with the results from the Moore cascade flow program. The agreement is excellent. Fig. 14 shows a comparison of the calculated and measured velocity profiles at two locations in the duct. The agreement is good at x=2.87 m, however, the calculated boundary layer at x=3.40 m is thinner than the measurements. It is noteworthy that the program has been able to calculate an essentially incompressible flow (M<0.075).

TEST CASE # 4

Turbulent flow in Sajben's transonic diffuser [5,6] has been calculated. The diffuser geometry (Model G) is shown in Fig. 15; the throat height was 44 mm and the ratio of the exit height to throat height was 1.5. Fig. 15 also shows the computational grid which had 83 points in the axial direction and 16 points across the flow. The development of a turbulent boundary layer was modelled on the curved surface, while the flat wall was treated as inviscid.

For the calculation, the ratio of the exit static pressure to the inlet total pressure was 0.8. This results in transonic flow in the diverging portion of the duct with a Mach number of approximately 1.235 upstream of a nearly normal shock. In the experiment, the flow remained fully-attached throughout the diffuser at this test condition. Since the code has not yet been developed to handle reverse flow an increased turbulent viscosity was used to avoid transient recirculation zones. In particular , a fixed minimum value for du/dy (60000 rad/s) was used to calculate the turbulent viscosity. The calculation then also gave a fully-attached turbulent flow.

Fig. 16 shows a comparison of the measured and calculated wall static pressure distributions on the curved wall. In the calculations, the shock is located upstream of the measured location, at $x/h^* = 1.2$ compared with $x/h^* = 1.4$. The calculated shock location is not sharp and further work is planned to improve shock capturing.

A comparison of the velocity profiles at three axial locations along the duct is shown in Fig. 17. The agreement is very good, especially downstream of the shock. It may be noted that the present calculations give much better agreement with the measured velocity profiles than the calculations of reference 6, shown as the solid lines.

Fig. 18 compares the measured and calculated total pressure loss for this operating point; the calculation underestimates the losses by about 20%. This lower value may be because the boundary layer on the flat wall was not included in the calculations and may also be due to the slightly weaker shock in

the calculation.

SUMMARY

The extensions to the explicit finite-volume time marching method have made possible the calculation of laminar and turbulent flows in ducts. The extensions can be summarized as follows:

1. non-uniform grid spacing in the transverse direction

2. a multi-volume method for pressure changes in the boundary layer

3. transverse upwind differencing

4. different updating procedure for the density and the pressure

5. a Prandtl mixing length model for the turbulent shear stresses.

These extensions have allowed the finite-volume method to calculate laminar and turbulent flow for a wide range of freestream Mach numbers(0.075 - 1.20) and geometries. For transonic flow in Sajben's diffuser, the calculated overall total pressure loss was in reasonable agreement with the measured

value. The results suggest that calculations of viscous flow in turbomachinery blade rows will be possible using the finite volume time marching method and that these calculations can model the losses.

REFERENCES

1. Nicholson,S. ,"Development of a Finite Volume Time Marching Method," V.P.I. & S.U. Turbomachinery Research Group Report No. JM/85-3, February 1985.

2. Denton, J.D., "An Improved Time Marching Method for Turbomachinery Calculations," ASME Paper 82-GT-239.

3. Moore,J. and Moore, J.G., "Calculation of Five Turbulent Flows Using the Moore Cascade Flow Program," 1980-81 AFOSR-HTTM-Stanford Conference on Complex Turbulent Flows, Volume III, 1982.

4. Kline,S.J. ,Cantwell, B.J., and Lilley,G.M.,"Complex Turbulent Flows Computation-Experiment," 1980-81 AFOSR-HTTM-Stanford Conference on Complex Turbulent Flows, 1982.

5. Bogar, T.J., Sajben, M. and Kroutil, J.C., "Characteristic Frequency and Length Scales in Transonic Diffuser Flow Oscillations," AIAA Paper 81-1291.

6. Liou, M.S., Coakley, T.J., and Bergmann, M.Y., "Numerical Simulation of Transonic Flow in Diffusers," AIAA Paper No. 81-1240 (June 1981)

Continuity

$$\Delta\rho = \sum_n (\rho\vec{V}\cdot d\vec{A})\ \Delta t/\Delta V$$

X-momentum

$$\Delta(\rho V_x) = \sum_n (P dA_x + \rho V_x \vec{V}\cdot d\vec{A} - \mu_{eff}\frac{\partial V_x}{\partial y} dA_y)^{*}\ \Delta t/\Delta V$$

Y-momentum

$$\Delta(\rho V_y) = \sum_n (P dA_y + \rho V_y \vec{V}\cdot d\vec{A})\ \Delta t/\Delta V$$

Energy

$$T_o = \text{constant}$$

Equation of State

$$P = \rho RT$$

* this is the only viscous term presently modeled

Table 1 Governing Equations

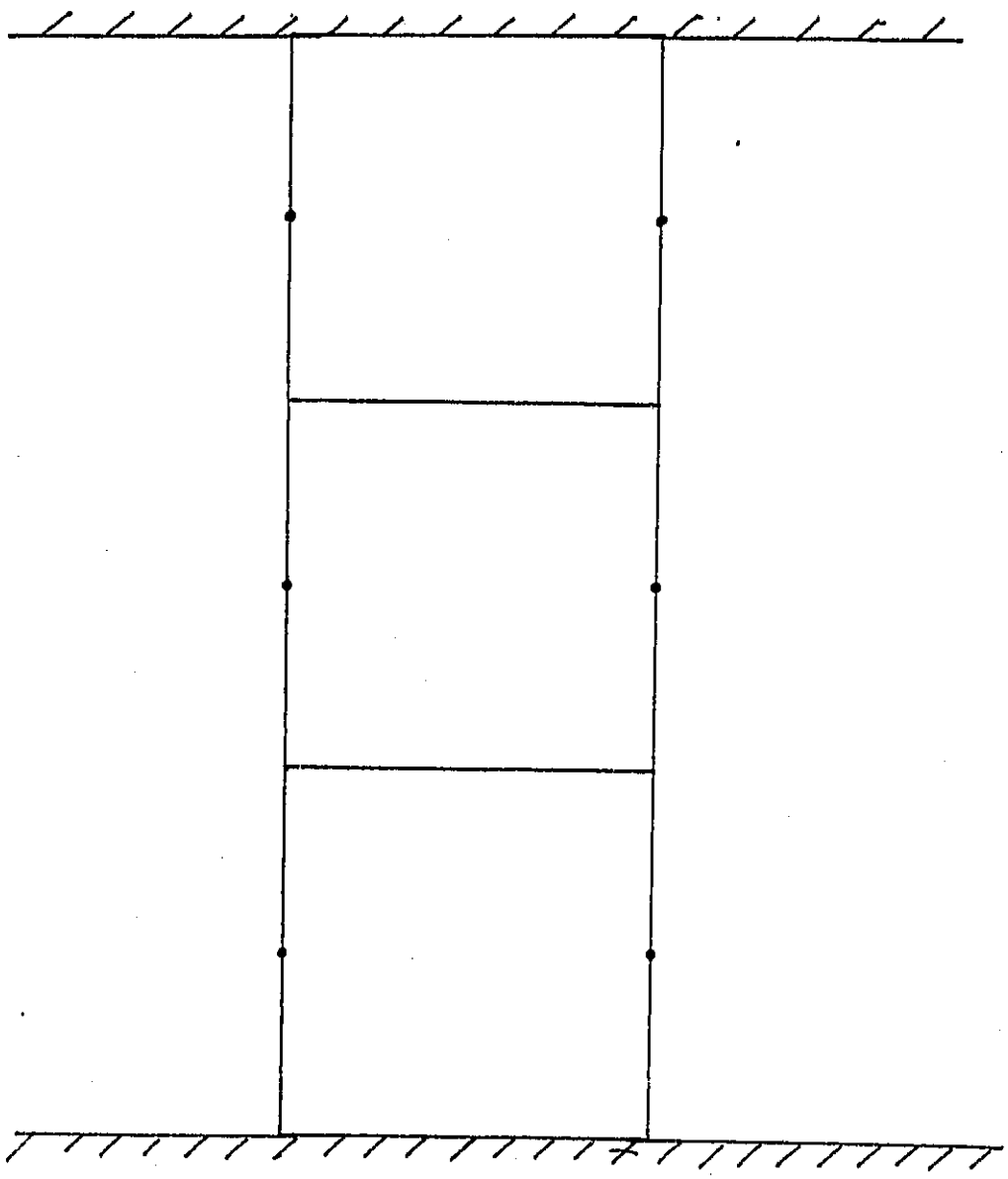

Fig. 1 New Control Volumes

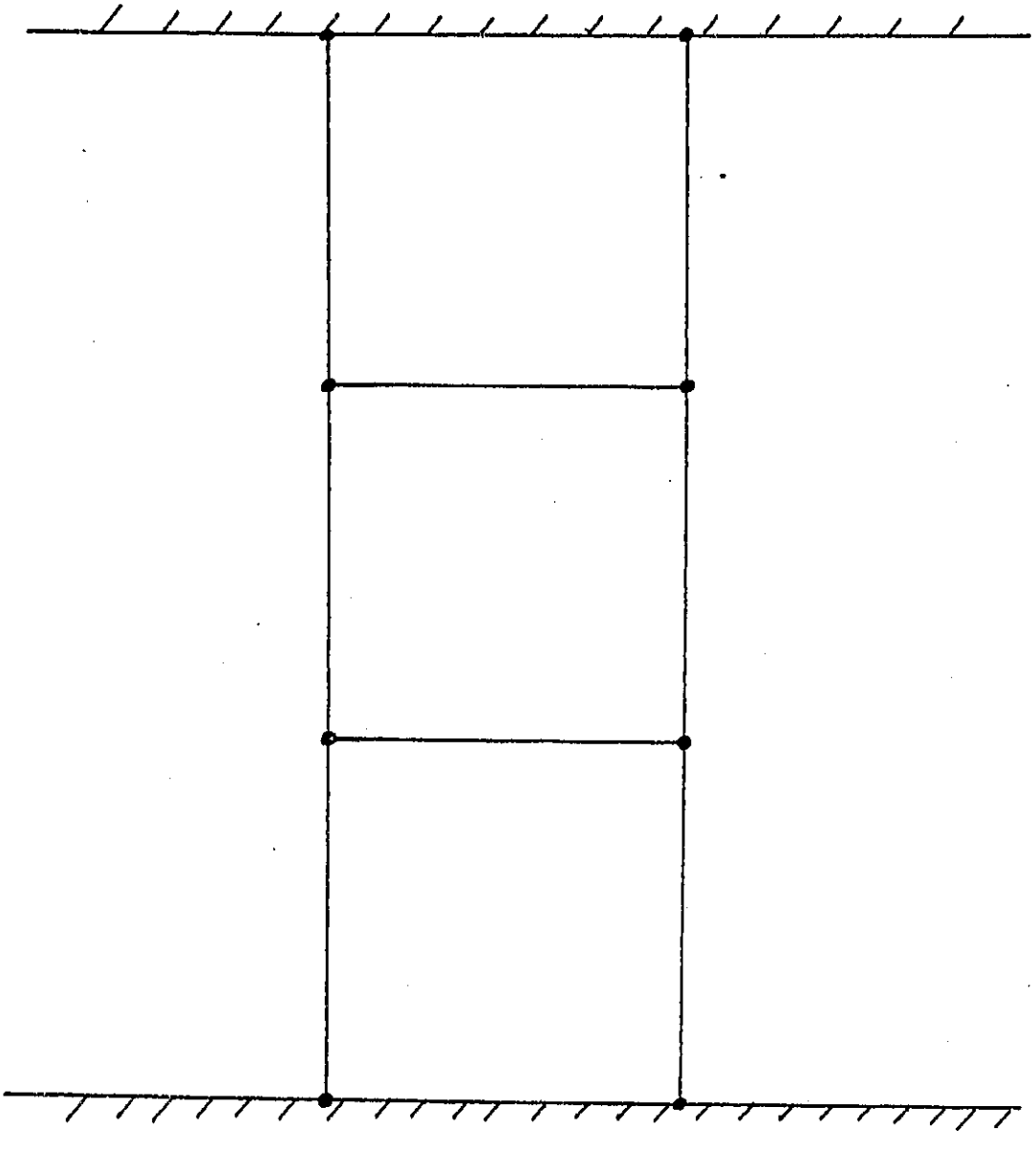

Fig. 2 Typical Control Volumes Used By Denton (2)

Table 2 Ratio of Time Steps for 1-D Compressible Flow

M	$\frac{\%\ \text{velocity change}}{\%\ \text{pressure change}}$	$\frac{\text{momentum time step}}{\text{continuity time step}}$
0.02	1670	800
0.10	79	72
0.80	1.1	2.1
1.00	0.7	1.7

Table 3 Prandtl Mixing Length Turbulence Model

- $\mu_T = \rho \ell^2 \frac{du}{dy}$
- in the boundary layer

$$\ell = \text{smaller of} \quad 0.41\, y \quad \text{or} \quad 0.08\, \delta$$

- in .41 y region $\ell = 0.41\, y\, (1 - \exp^{\left(\frac{-y(\rho\tau)^{1/2}}{26\mu_\ell}\right)})$

- between the near wall point and the wall

$$\mu_{eff} = \sqrt{\mu_\ell (\mu_\ell + \mu_T)}$$

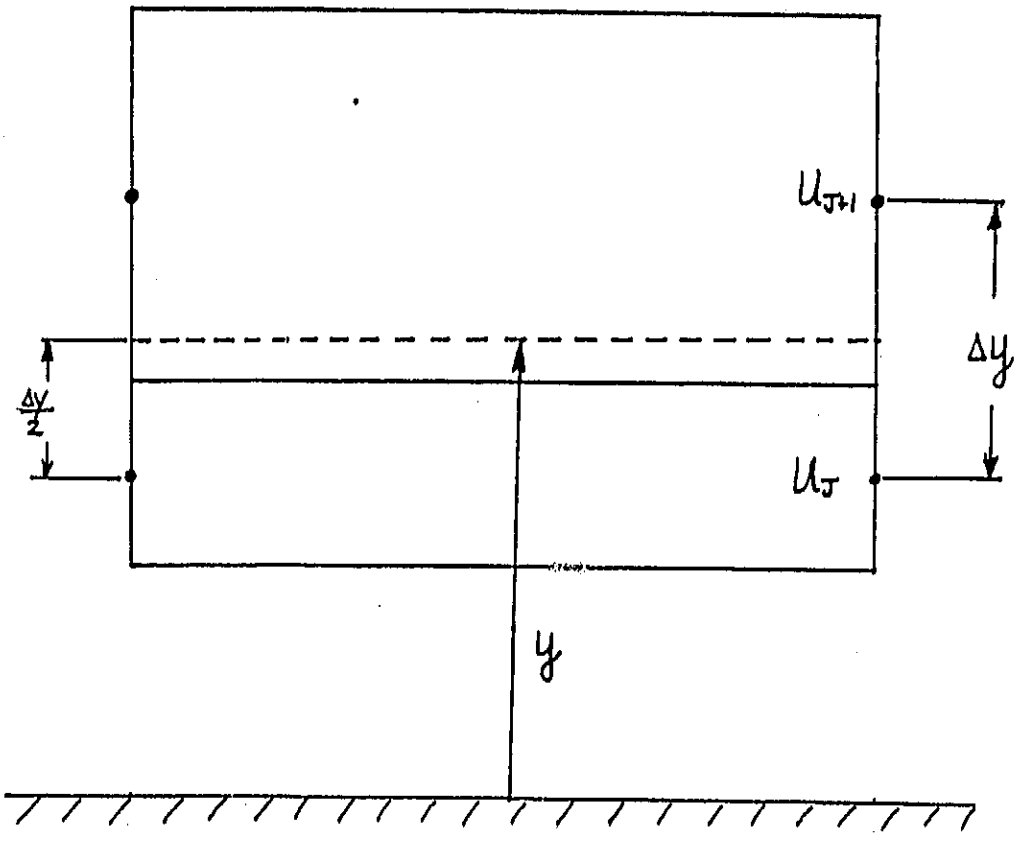

Fig. 3 Shear Stresses For Non-Uniform Grid

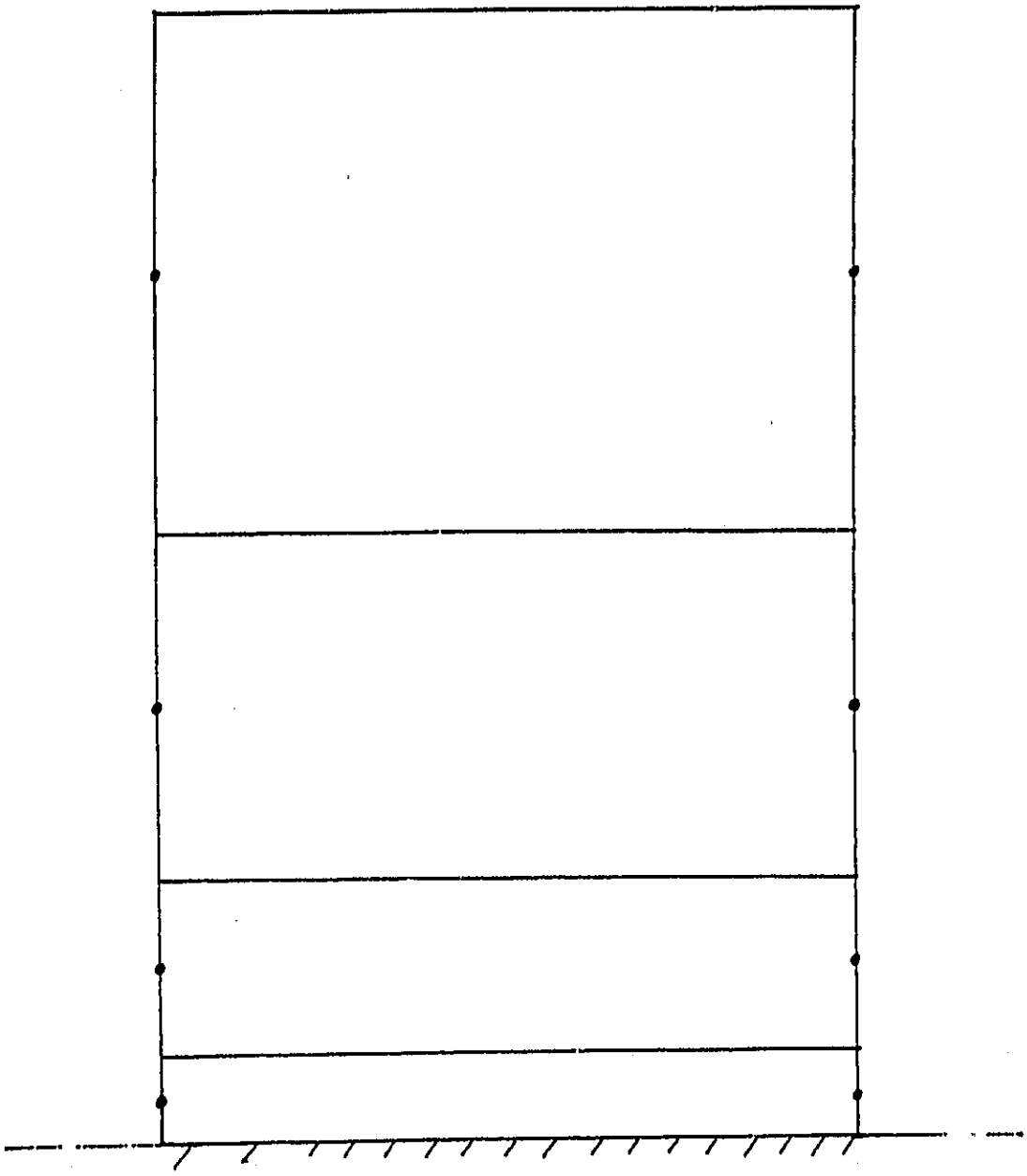

Fig. 4 Non-Uniform Grid in the Boundary Layer

Table 4 Typical Transverse Distribution of Grid Points, y/h

Turbulent Boundary Layer δ = .09 h	Laminar Boundary Layer δ = .15 h
h= duct height	
.0005	.015
.0020	.045
.0050	.075
.0110	.105
.0230	.135
.0470	.175
.0950	.225
.1910	.275
.3080	.300
.4150	.334
.5210	.438
.6280	.550
.7340	.650
.8410	.750
.9470	.850
	.950

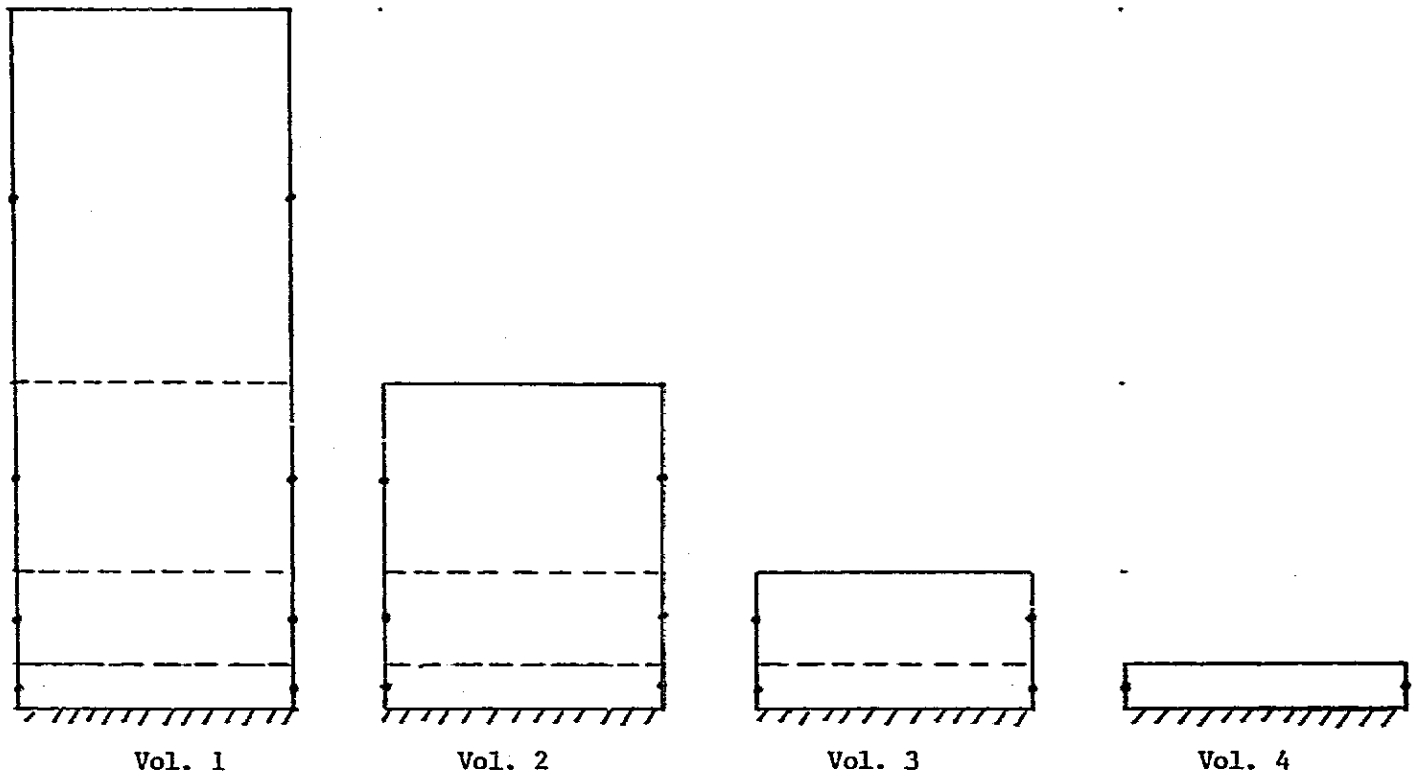

Fig. 5 Multi-Volume Method For Pressure Changes in the Boundary Layer Using Successively Smaller Control Volumes

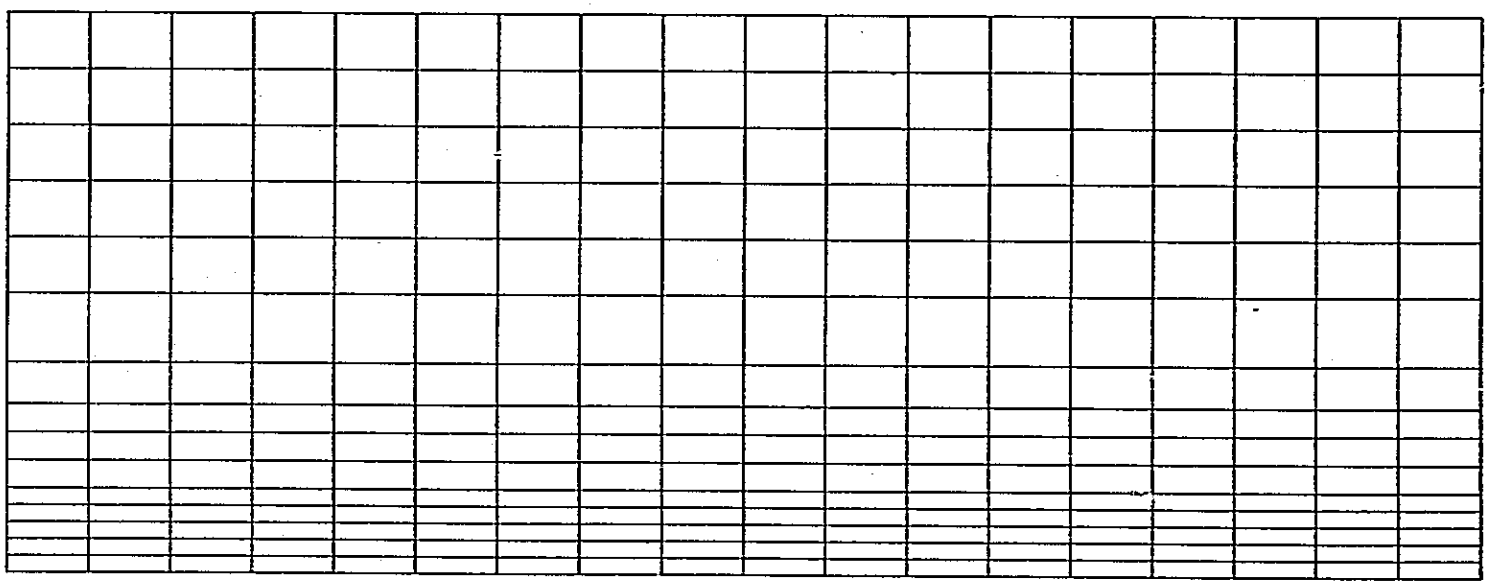

Fig. 6 Geometry and Grid For Zero Pressure Gradient Test Case

Fig. 7 VELOCITY PROFILE ON FLAT PLATE

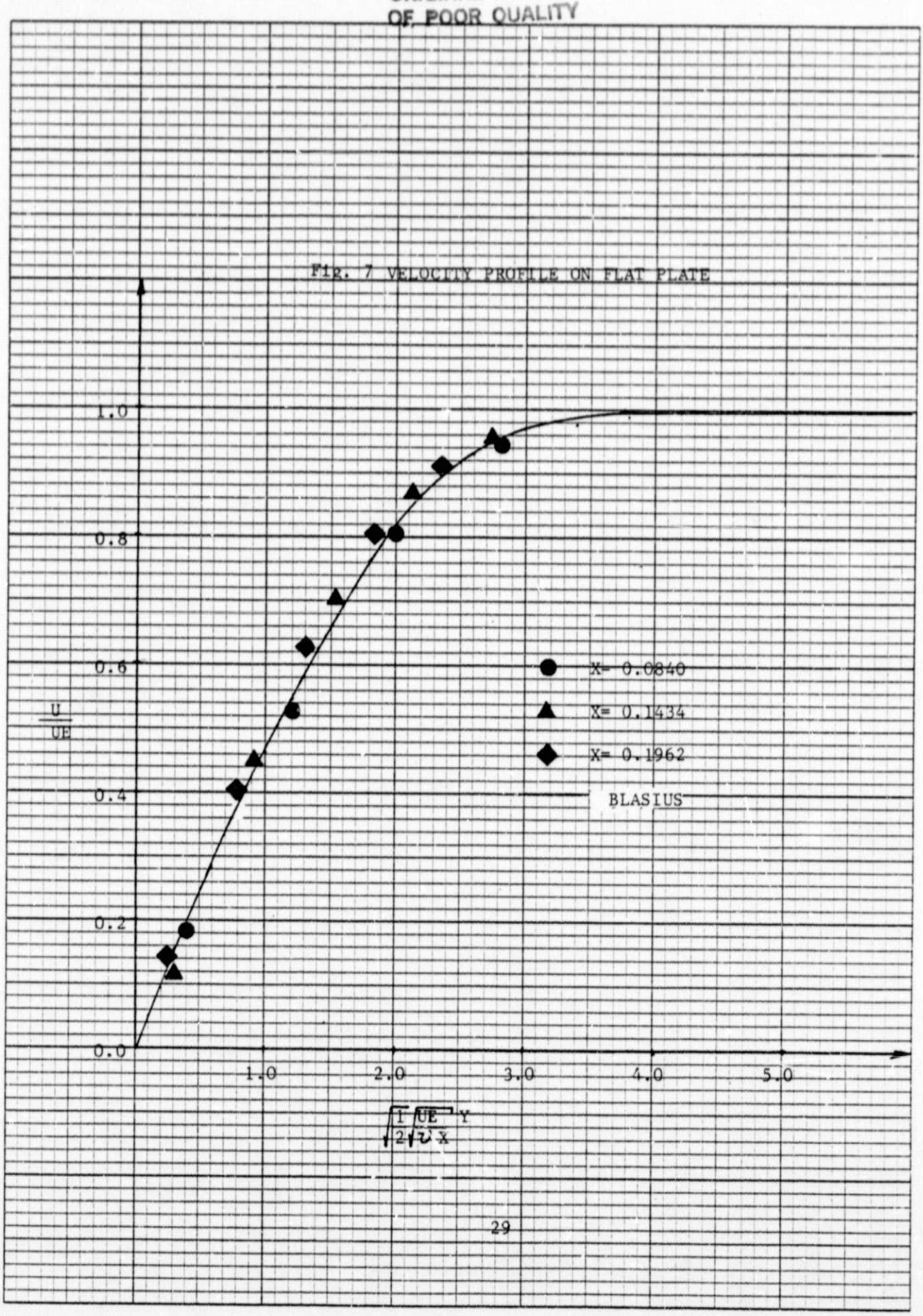

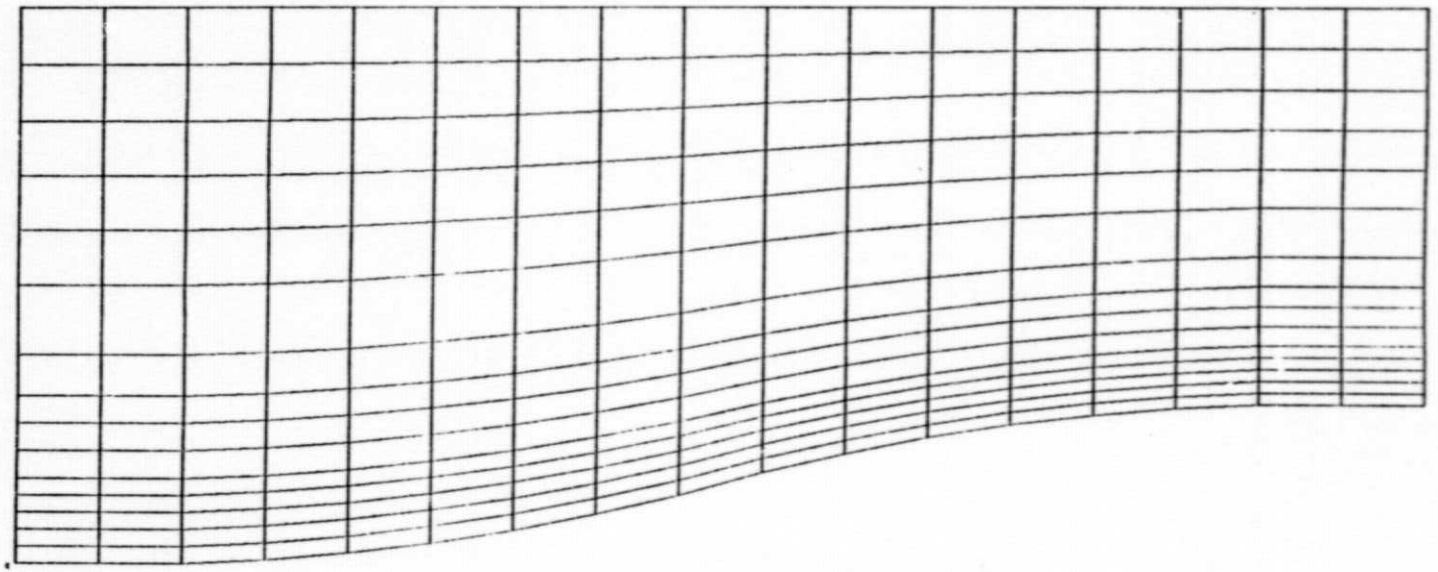

Fig. 8 CONVERGING NOZZLE GEOMETRY AND GRID

Fig. 9 VELOCITY PROFILE IN CONVERGING NOZZLE

(LAMBDA = 0.0)

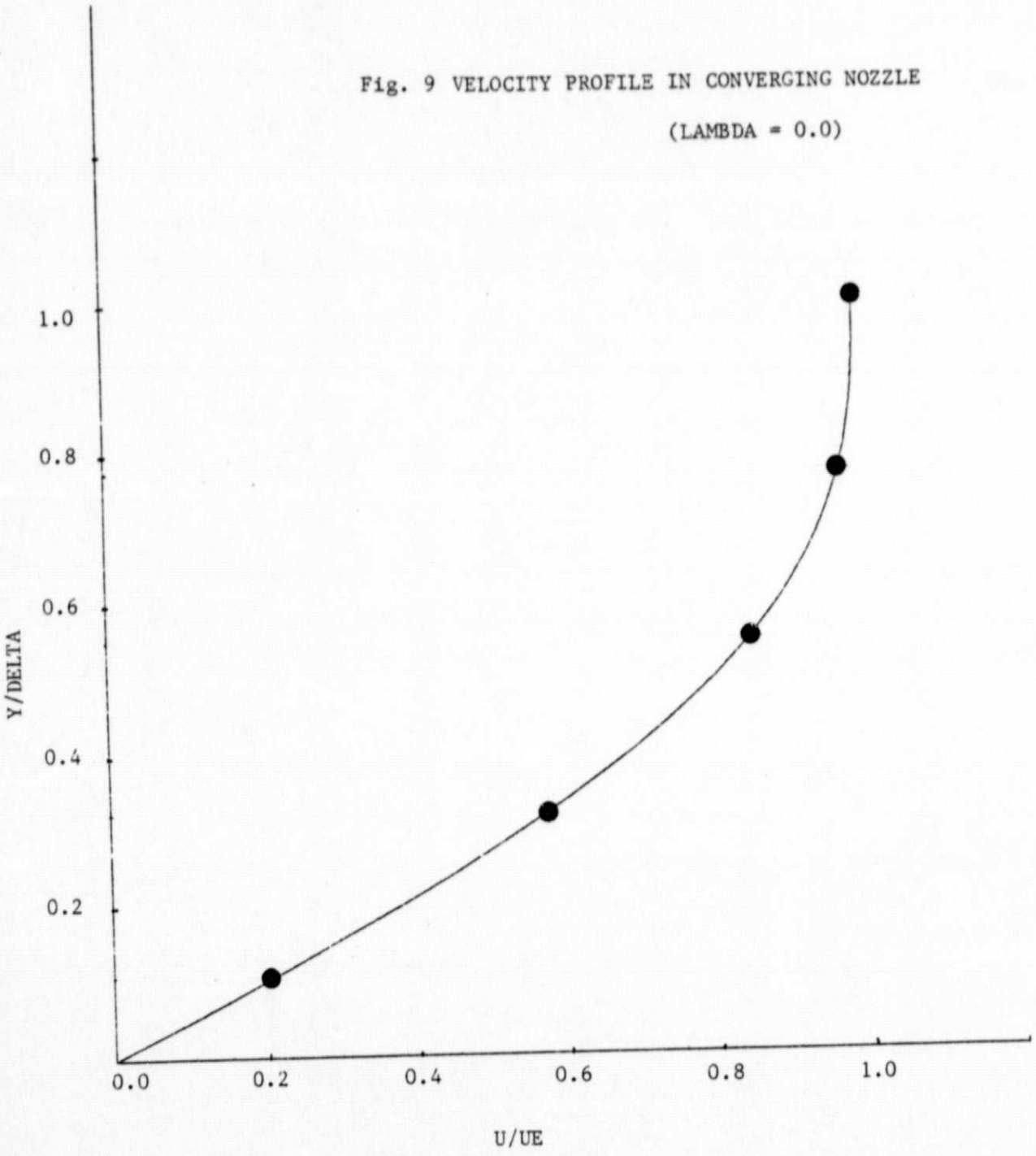

Fig. 10 VELOCITY PROFILE IN CONVERGING NOZZLE

(LAMBDA = 9.1)

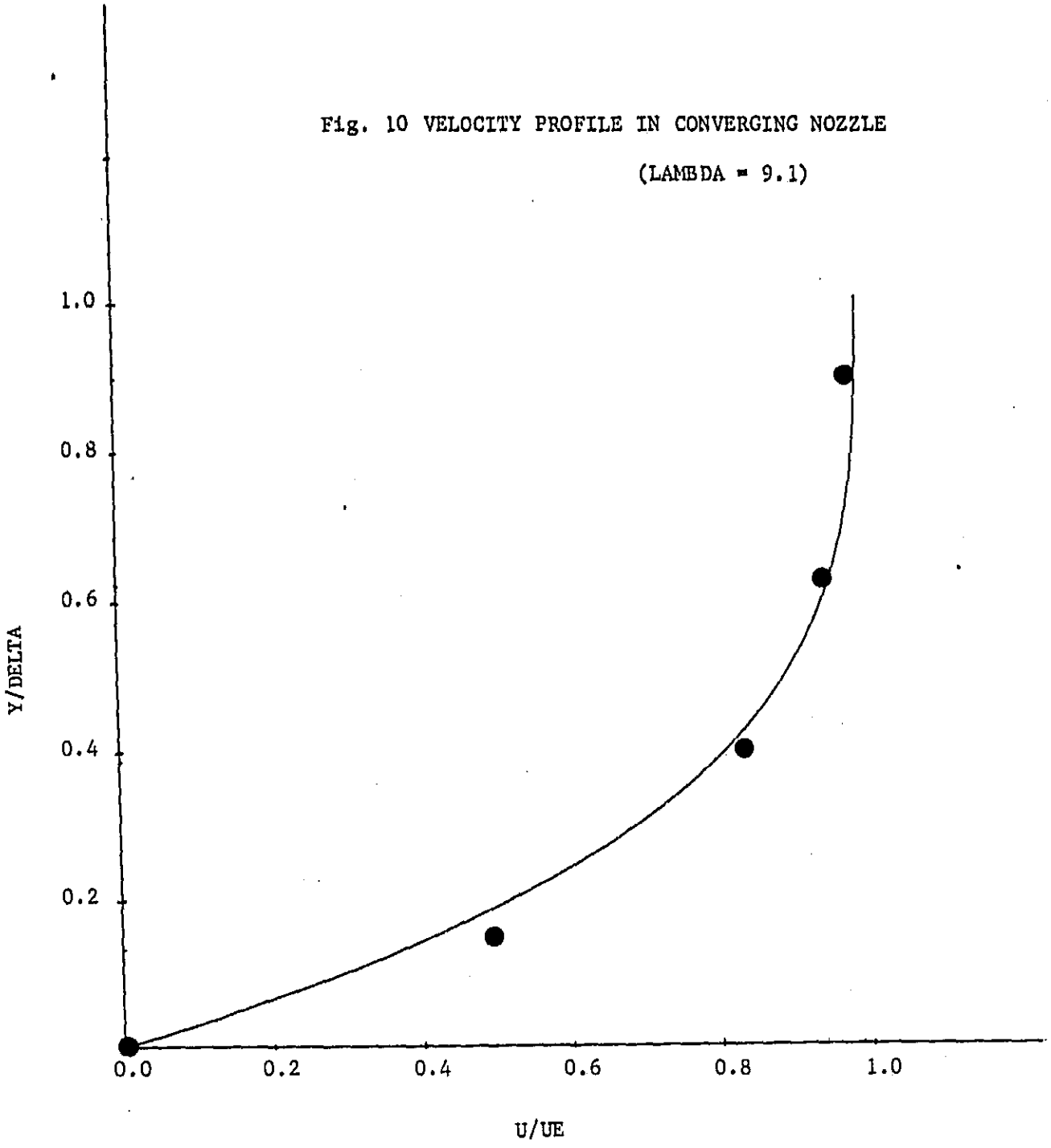

Fig. 11 VELOCITY PROFILE IN CONVERGING NOZZLE

(LAMBDA = 2.0)

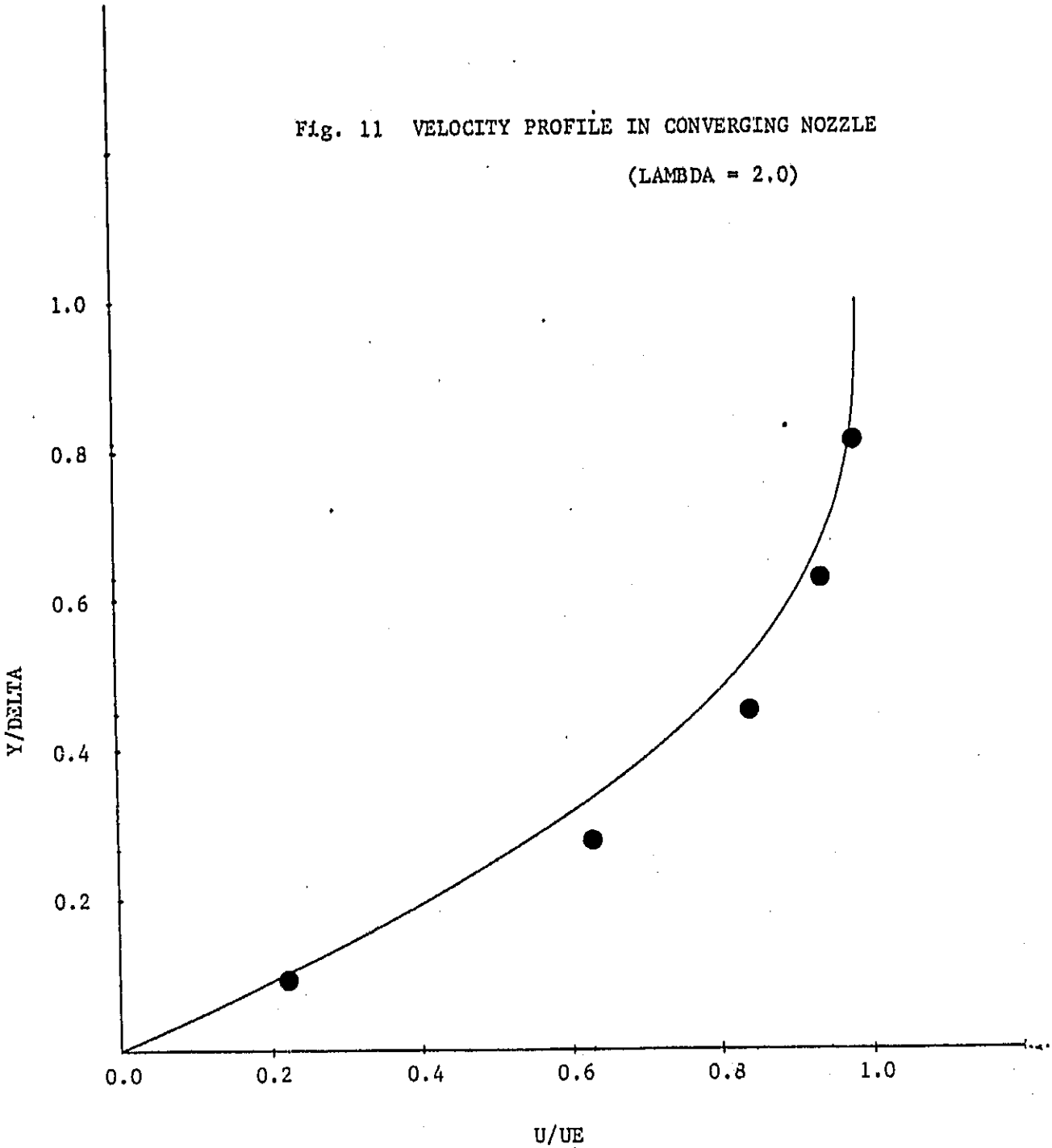

Fig. 12 GEOMETRY AND GRID FOR SAMUEL AND JOUBERT

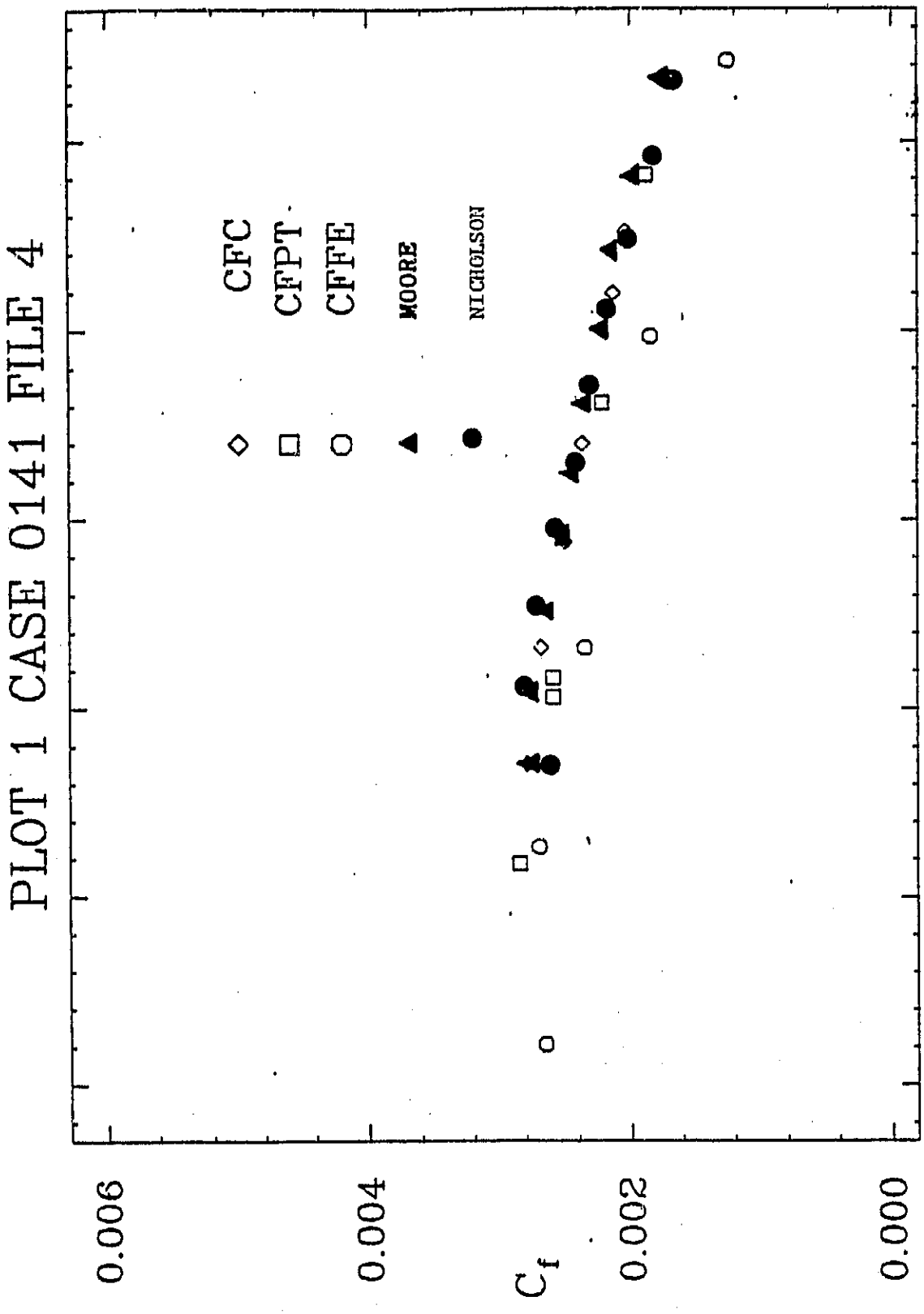

Fig. 13 Skin Friction Coefficient For Samuel and Joubert

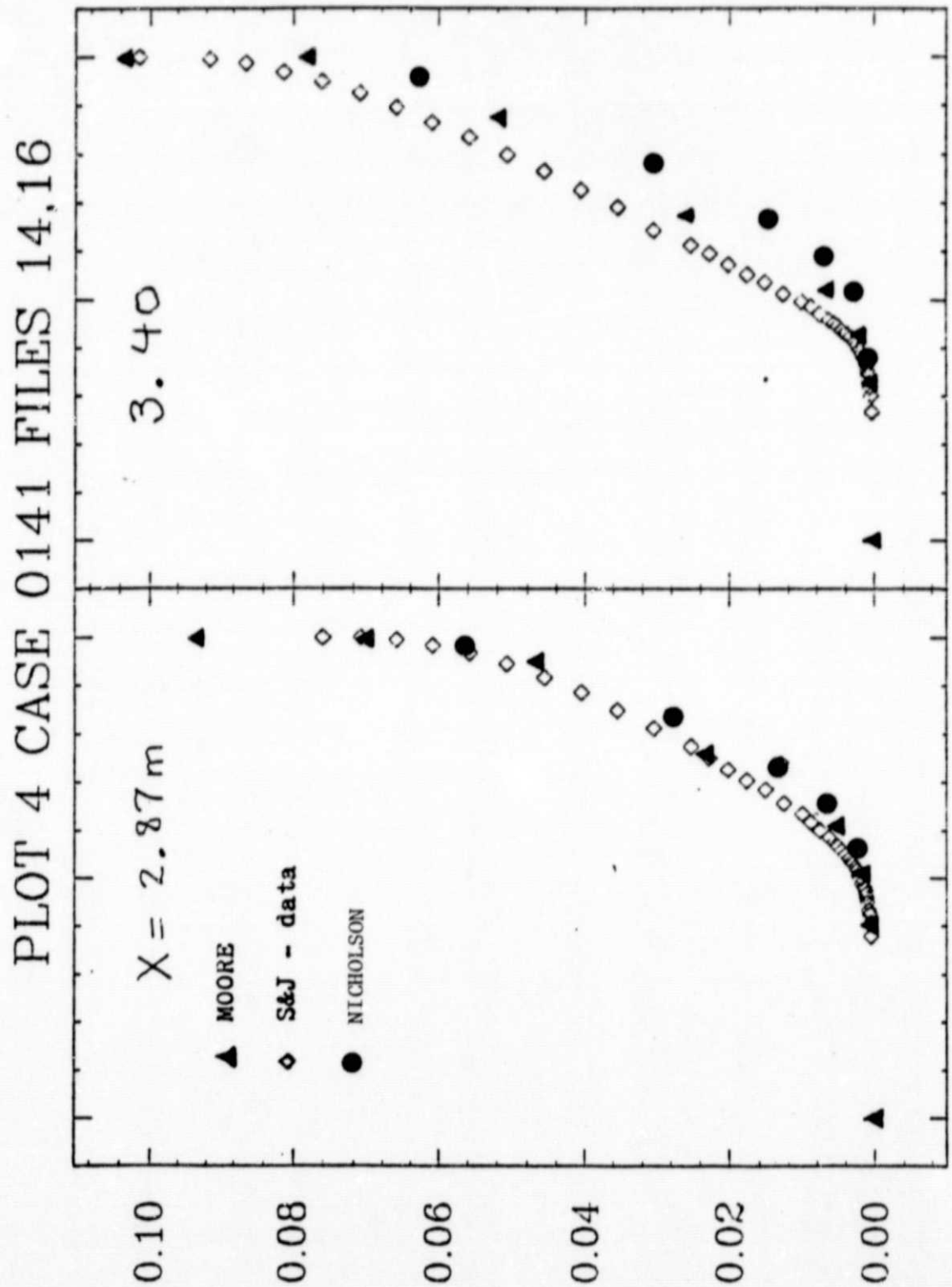

Fig. 14 Velocity Profiles for Samuel and Joubert

Revised 12/30/8

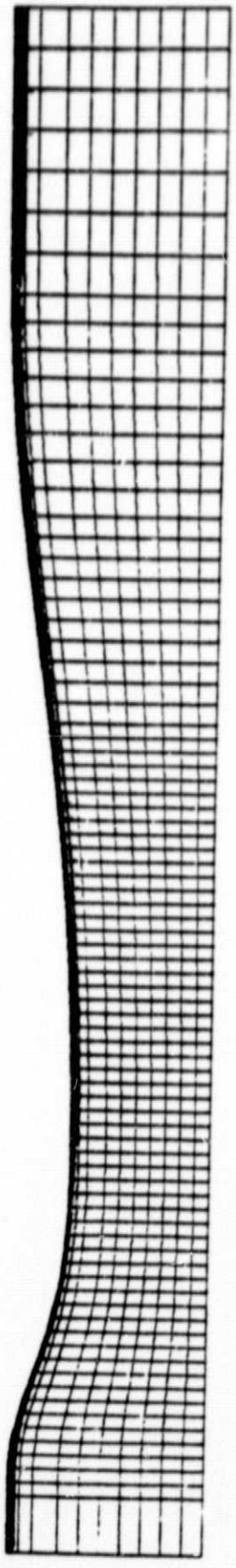

Fig. 15 Geometry and Grid for Sajben's Diffuser

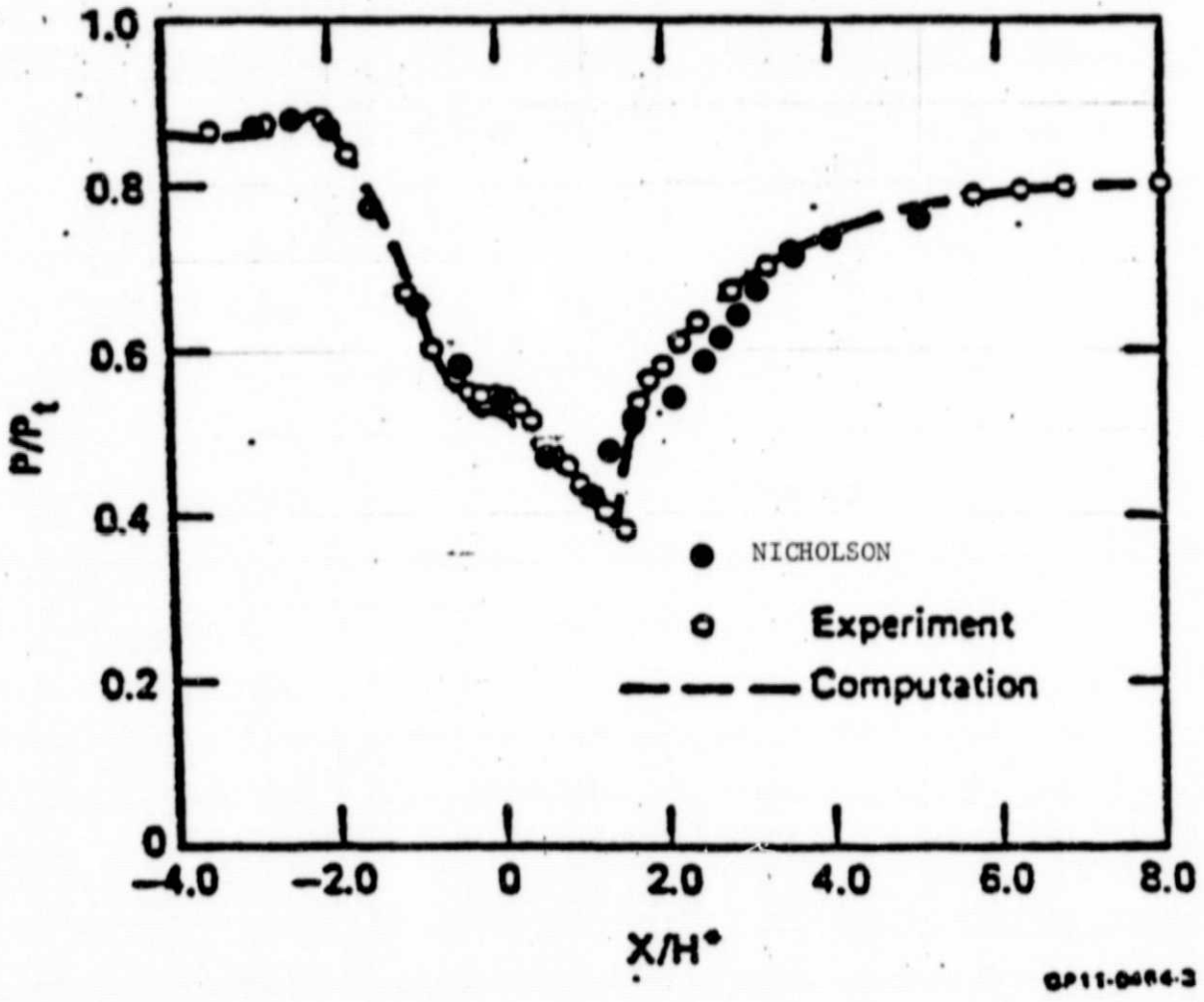

Fig. 6 Surface pressure distribution on upper wall. Model G, $R_p = 0.8$. ($\gamma_\infty = 10/9$, $Pr_k = Pr_\omega 2 = 1.0$)

Fig. 16 Wall Static Pressure Distribution for Sajben's Diffuser

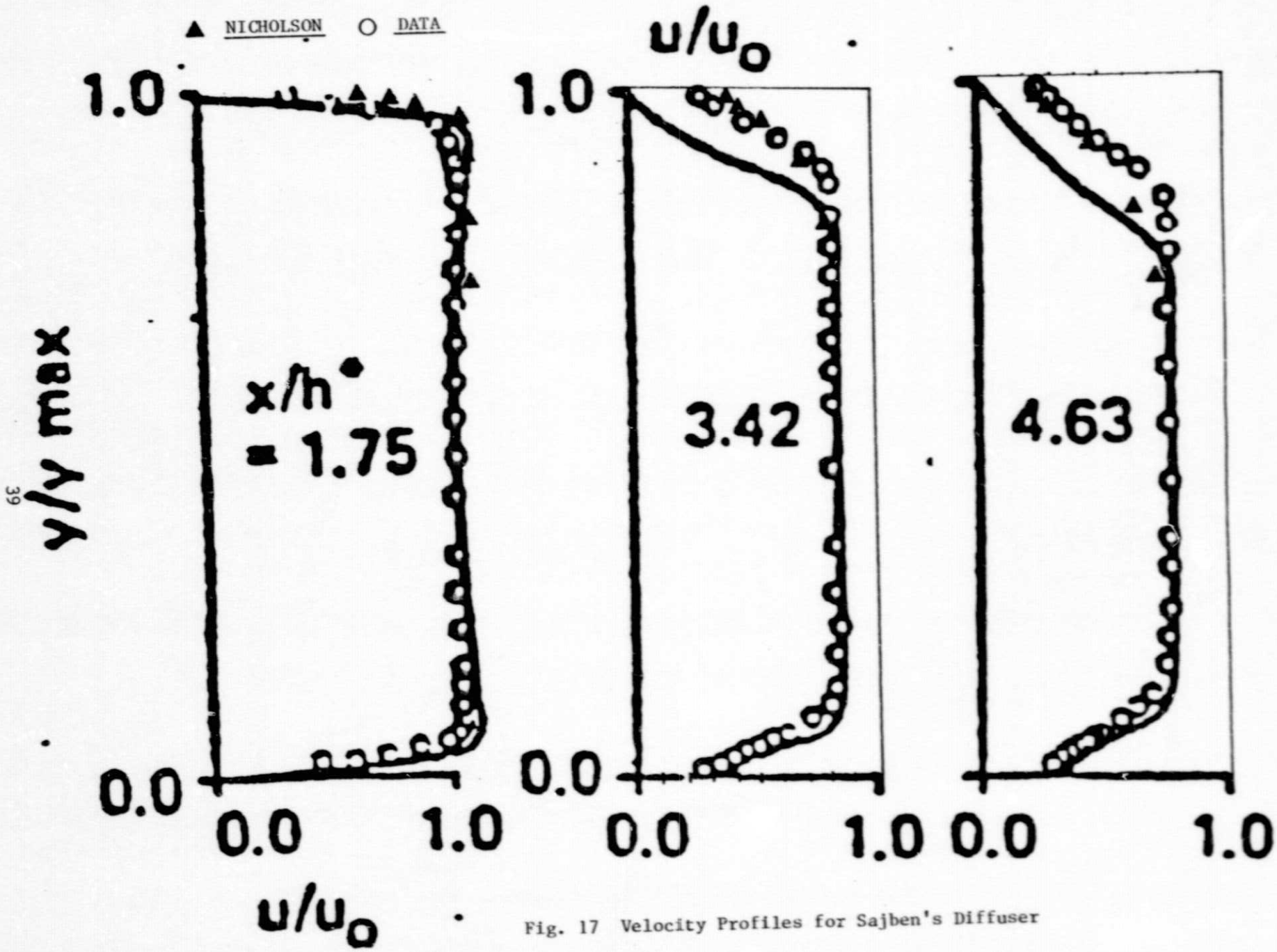

Fig. 17 Velocity Profiles for Sajben's Diffuser

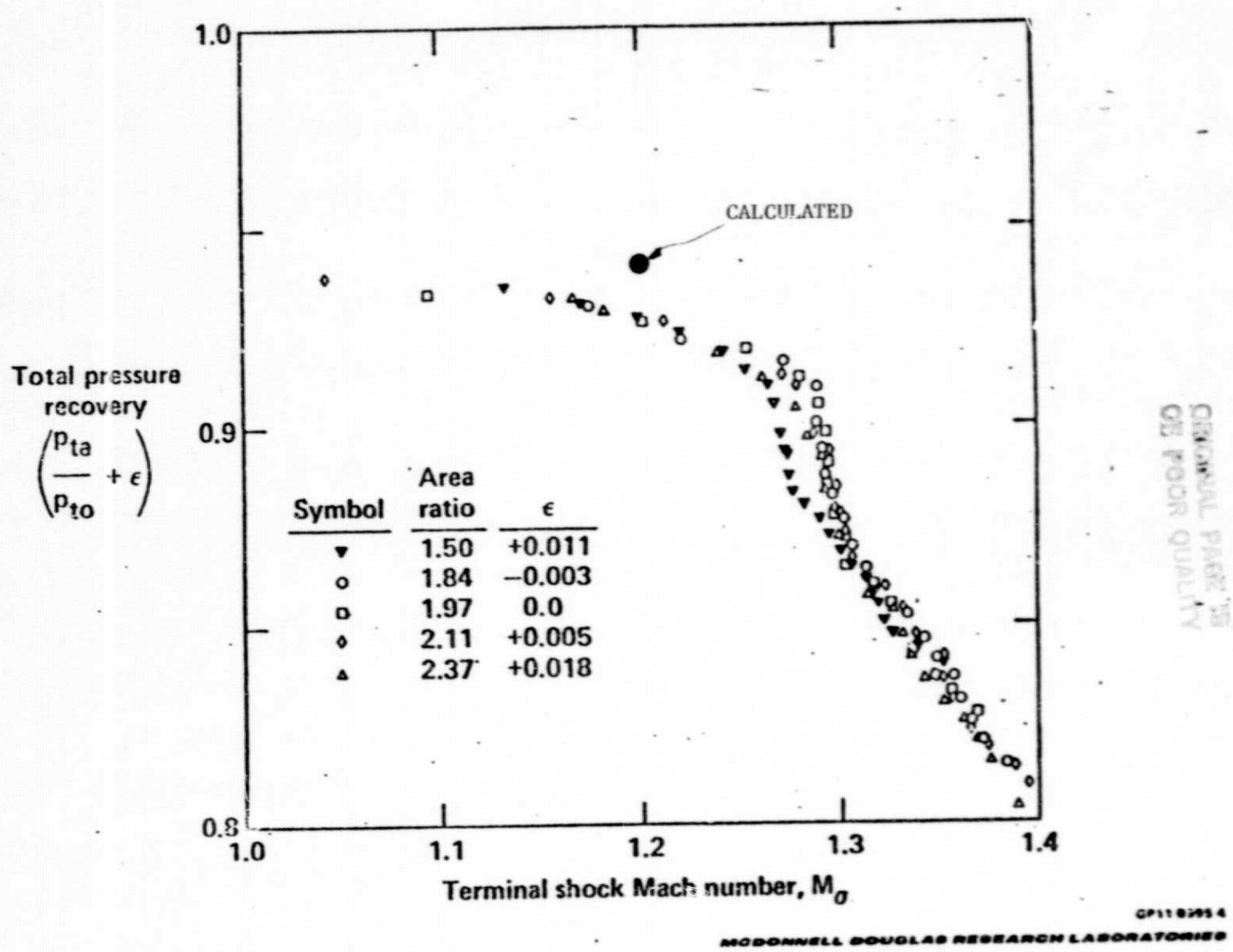

Fig. 18 Total Pressure Loss Comparison For Sajben's Diffuser